Applied Physics Letters

Energy storage properties of polyimide/$BaTiO_3$ nanocomposite films and their breakdown mechanism in a wide content range

Cite as: Appl. Phys. Lett. **115**, 213901 (2019); https://doi.org/10.1063/1.5115766
Submitted: 21 June 2019 . Accepted: 01 November 2019 . Published Online: 18 November 2019

Jiasheng Ru, Daomin Min, Michael Lanagan, Shengtao Li, and George Chen

Applied Physics Letters ARTICLE scitation.org/journal/apl

Energy storage properties of polyimide/$BaTiO_3$ nanocomposite films and their breakdown mechanism in a wide content range

Cite as: Appl. Phys. Lett. **115**, 213901 (2019); doi: 10.1063/1.5115766
Submitted: 21 June 2019 · Accepted: 1 November 2019 ·
Published Online: 18 November 2019

View Online Export Citation CrossMark

Jiasheng Ru,[1,2] Daomin Min,[1] Michael Lanagan,[2,a)] Shengtao Li,[1,a)] and George Chen[1]

AFFILIATIONS

[1]State Key Laboratory of Electrical Insulation and Power Equipment, School of Electrical Engineering, Xi'an Jiaotong University, Xi'an, Shaanxi 710049, People's Republic of China
[2]Materials Research Institute, The Pennsylvania State University, University Park, Pennsylvania 16802, USA

[a)]**Authors to whom correspondence should be addressed:** mxl46@psu.edu and sli@mail.xjtu.edu.cn

ABSTRACT

Polyimide (PI) has excellent dielectric properties with superior thermal stability, and it is considered as a promising polymer dielectric for energy storage capacitors. Here, we studied the energy storage properties of PI composite films with $BaTiO_3$ (BT) nanoparticles in a wide content range. Benefiting from the high breakdown strength (520 kV/mm), the nanocomposite filled with 0.05 wt. % of BT exhibits an increased energy density of 4.51 J/cm^3 at room temperature and keeps a good thermal stability (3.22 J/cm^3 at 100 °C). Additionally, trap properties of the nanocomposites and their effect on breakdown strength were studied by thermally stimulated depolarization current. It was found that the dominant trap parameter on breakdown strength variation, with the increase in the BT content, is correlated with deep traps, deep and shallow traps especially their depths, and shallow trap density. Then, a physical quantity of average trap depth was introduced, the value of which decreases from 0.81 eV to 0.44 eV as the BT content increases to 50 wt. %, and a clear correspondence was discovered between the average trap depth and breakdown strength.

Among the various electrical energy storage technologies, polymer film capacitors are strongly attractive because of their flexibility, unique self-healing ability, high operating voltage, and large power density. They have significant applications in many fields[1–5] such as modern electronics, electric vehicles, and power system. However, the low energy density of capacitor films hinders the full display of their potential in many applications. For example, the energy density of biaxially oriented polypropylenes, the most common dielectric in commercial film capacitors, is only 1–2 J/cm^3.[6,7]

Polyimide (PI) is a promising polymer dielectric for energy storage capacitors owing to its excellent electrical properties and superior thermal stability. To improve its energy density, PI/ceramic nanocomposites,[8–11] PI composites containing conductive nanofillers,[12–14] and three-phase PI nanocomposites by means of direct mixing[15–17] or core-shell structure[18–20] were investigated in the last decade. Most of these works focused on dielectric and energy storage properties, with less attention to the breakdown mechanism. Some relevant electrical studies were performed in the last several years, but they mainly focused on the relationship between partial trap parameters (usually deep trap depth or density) and breakdown strength at a low content of nanoparticles.[3,21–23]

Recently, researchers introduced small amounts of one-dimensional (1D) ceramic nanofillers (about 1–5 vol. %) into a polymer matrix and obtained enhanced energy density and breakdown strength;[20,24–26] however, these properties were weakened with the same content as the corresponding nanoparticles.[25,26] The enhancement is attributed to the increased migration paths of carriers caused by those 1D nanofillers vertical to the applied electric field.[27] However, in comparison with nanoparticles, there are still some problems in well-controlled fabrication of 1D nanostructures.[28–30] Furthermore, the 1D nanofillers close to the through-plane direction will provide conductive paths for carriers. Even though several research studies have been performed on the aligned 1D nanostructures in the polymer matrix recently,[27,31] it is still challenging to develop a universal and effective alignment technology. All of these process challenges may severely affect the stability and reliability of polymer nanocomposites' electrical properties. Alternatively, according to the multiregion structure theory,[32] it is also possible to enhance the breakdown strength of

the polymer matrix by introducing a much lower content of ceramic nanoparticles.

In this paper, the dielectric, breakdown, and energy storage properties of PI/$BaTiO_3$ (BT) nanocomposites were studied, in which the maximum breakdown strength, breakdown stability, and energy density were found at a very low content of BT nanoparticles. Moreover, trap properties of the nanocomposites and their effect on breakdown strength variation were explored by the thermally stimulated depolarization current (TSDC) technique. A physical quantity of average trap depth was also defined to assist in analyzing their relationship with dielectric failure more effectively.

PI/BT nanocomposite films with different mass fractions were fabricated through the *in situ* polymerization method.[8] The typical thickness of PI/BT nanocomposite films was about 25 μm. The dc breakdown strength was measured in transformer oil, with a sphere-sphere electrode fixture of diameter 25 mm and a voltage ramp of 0.5 kV/s. Before further electrical measurements, gold electrodes of 8 mm diameter on the high voltage side and 11 mm diameter on the low voltage side were sputtered on film surfaces. The dielectric tests were performed using an impedance analyzer (4294A, Agilent) at room temperature. The TSDC spectra were measured using a HP 4140B pA meter, and the measurement parameters are set as follows: poling temperature: 120 °C, poling electric field: 20 kV/mm, poling time: 30 min, cooling rate: 15 °C/min, and heating rate: 3 °C/min. The detailed operation procedure on the TSDC measurements is described in Ref. 33. The electric displacement-electric field (D-E) loop tests were carried out at 100 Hz on an in-house developed apparatus.

Figure 1(a) shows the relative permittivity (ε_r) of PI/BT nanocomposites. The permittivity of the composites, filled with the BT content lower than 5 wt. %, is close to that of Pure PI. However, it is greatly improved at a higher content. For instance, at 100 Hz, the relative permittivities of PI nanocomposites with 20 wt. %, 30 wt. %, and 50 wt. % of BT are 5.2, 6.7, and 10.3, respectively, which are 1.3, 1.6, and 2.5 times larger than Pure PI's value. In addition to the BT particles, the boundary between ceramic nanofillers and the polymer matrix (viz., interface) also contributes to the permittivity enhancement, which was demonstrated in Refs. 9 and 34 through the obvious difference between the calculated and experimental permittivity values. The dielectric loss ($\tan\delta$) of the PI/BT nanocomposites in Fig. 1(b) is smaller than 0.02 over the frequency range of 10^2–10^6 Hz. At low frequencies, loss increases with the increase in the BT content except at 0.05 wt. %, which is governed by the change of their conductivity. Loss peaks are found in pure PI and its nanocomposites at a frequency of about 5×10^5 Hz, which are attributed to the coupled water molecules and limited motions of carbonyl groups.[35]

In order to study the breakdown property of PI/BT nanocomposites more accurately, 28 test points were taken for each sample during the dc breakdown measurement. Then, the results were analyzed by a two-parameter Weibull distribution function,[36]

$$P_f(E_s, \beta) = 1 - \exp\left[-\left(\frac{E_m}{E_s}\right)^{\beta}\right], \quad (1)$$

where P_f is the cumulative probability distribution function; E_m is the experimentally measured breakdown strength in kilovolt per millimeter; the scale parameter E_s represents the breakdown strength at a probability of 63.2% in kilovolt per millimeter; and the shape parameter β characterizes the scatter of experimental data, i.e., the breakdown stability.

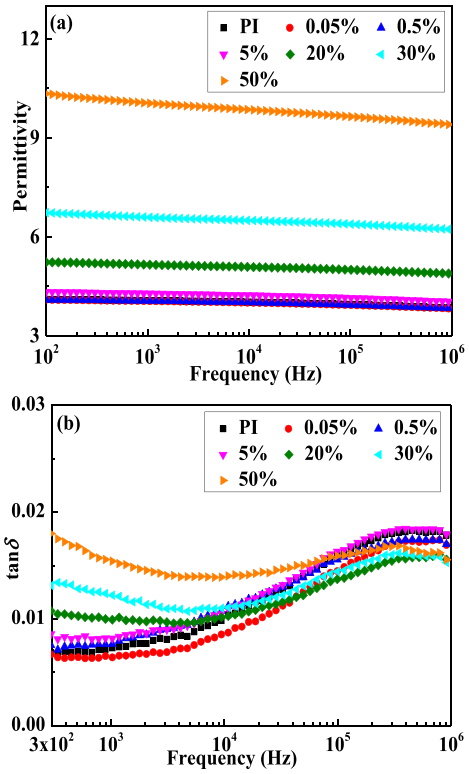

FIG. 1. Frequency dependence of (a) relative permittivity and (b) dielectric loss for the PI/BT nanocomposite.

Figure 2 shows the Weibull breakdown distributions of PI/BT nanocomposites. E_s initially increases with the BT content, and a maximum value of 520 kV/mm is reached at 0.05 wt. % and becomes

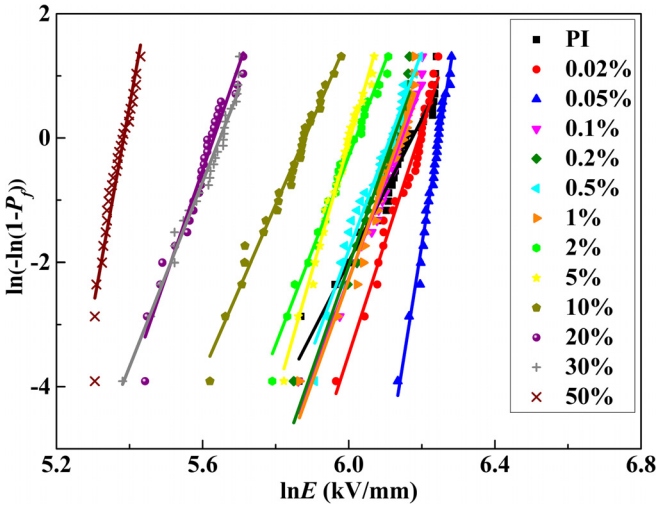

FIG. 2. Weibull breakdown distribution of PI/BT nanocomposite films.

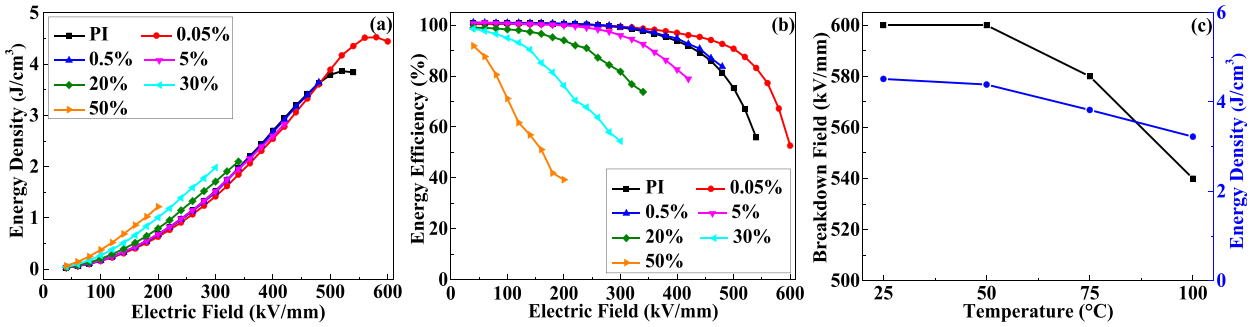

FIG. 3. (a) Energy density and (b) energy efficiency of PI/BT nanocomposites at the electric field from 40 kV/mm until breakdown occurred. (c) Breakdown field and energy density of the PI/BT (0.05 wt. %) nanocomposite at different temperatures.

comparable with that of pure PI (471 kV/mm) for nanofiller loading between 0.1 and 1 wt. %. For the nanocomposites with a higher content of BT, a dramatic reduction of E_s is observed. Meanwhile, β is also first enhanced, which is 11.5, 18.1, and 36.8 for pure PI, the nanocomposite with 0.02 wt. % of BT, and the nanocomposite with 0.05 wt. % of BT, respectively, and then fluctuates within 13.5–20.4 at a higher content. The local electric field in the nanocomposites with a high BT content increases significantly because of much shorter distances between the nanoparticles and the permittivity contrast between the polymer matrix and the ceramic nanofillers.[37,38]

The discharged energy density (U_e) and efficiency of PI/BT nanocomposites, which were calculated from the results of *D-E* loops, are presented in Fig. 3. Because of the increased permittivity, the energy density is obviously improved at a low electric field while the BT content is higher than 20 wt. %. However, their maximum energy density is restricted by the breakdown strength reduction. Benefiting from the higher breakdown field, the nanocomposite with 0.05 wt. % of BT exhibits an increased energy density of 4.51 J/cm^3 with the energy efficiency of 77% at room temperature. Meanwhile, as shown in Fig. 3(c), there is a good thermal stability. At 100 °C, its breakdown field and energy density are maintained at relatively high values of 540 kV/mm and 3.22 J/cm^3, respectively. For pure PI and all the nanocomposites, the energy efficiency obviously decreases with the increasing electric field due to the rising leakage current. Moreover, the breakdown field of all the samples is slightly higher than their dc breakdown strength because of the much faster voltage rise and much shorter voltage time.

The comparison between this work and the literature on PI nanocomposites is summarized in Table I. In the table, several U_e values are calculated from $1/2\varepsilon_0\varepsilon_r E_s^2$ (where ε_0 is the vacuum permittivity) instead of *D-E* loops, and hence their actual values should be some lower than the reported ones. As seen in most literature, ceramic nanofiller addition was effective in increasing ε_r but hard to maintain E_s. In this work, a relatively large U_e with high E_s was achieved. A large U_e was also achieved by introducing small loading of BT nanofibers in Ref. 25, however, the problem of in-plane alignment needs to be studied further for better breakdown stability.

The TSDC technique was used to understand the trap properties of the nanocomposites and their influence on the breakdown strength. Considering the limitation of the initial rise method, various heating rate methods, and other algorithms,[43] the general TSDC expression[33] was directly employed for the calculation of our TSDC measurement results, as shown in Fig. 4,

$$I(T) = \frac{Q_0}{\tau_0}\exp\left[-\frac{\mu_a}{k_B T} - \frac{1}{\gamma\tau_0}\int_{T_0}^{T}\exp\left(-\frac{\mu_a}{k_B T}\right)dT\right], \quad (2)$$

TABLE I. Comparison in relative permittivity ε_r, breakdown strength E_s, and discharged energy density U_e between this work and the literature.

Samples	ε_r and 1 kHz	E_s (kV/mm)	U_e (J/cm^3)	U_e method
10 vol. % BST-nps[10]	∼3.7	296	2.9	$\frac{1}{2}\varepsilon_0\varepsilon_r E_s^2$
40 vol. % BT-nps and 10 vol. % multi-walled carbon nanotubes[15]	∼780	31.9	4.77	$\frac{1}{2}\varepsilon_0\varepsilon_r E_s^2$
3 vol% BT and SiO_2-nfs[20]	∼4.4	346	2.31	$\frac{1}{2}\varepsilon_0\varepsilon_r E_s^2$
1 vol. % BT-nfs[25]	∼3.9	553	5.82	*D-E* loops
1 vol. % BT-nps[39]	∼3.4	∼300	∼1.6	*D-E* loops
2 vol. % BT-nws[40]	∼4.8	220	1.06	*D-E* loops
1 vol. % CCTO and TiO_2-nfs[41]	∼4.1	299	1.6	$\frac{1}{2}\varepsilon_0\varepsilon_r E_s^2$
5 wt. % platelike BNT[42]	∼14.5	141	1.24	$\frac{1}{2}\varepsilon_0\varepsilon_r E_s^2$
0.05 wt. % BT-nps (this work)	4.05	520	4.51	*D-E* loops

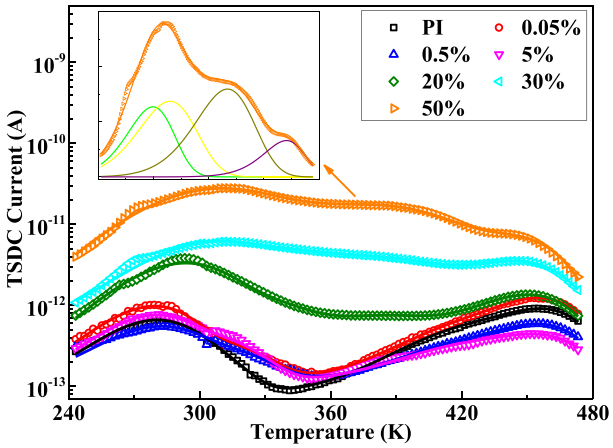

FIG. 4. Experimental (point) and fitting (line) TSDC curves of PI/BT nanocomposites.

$$\tau_0 = \frac{k_B T_m^2}{\gamma \mu_a} \exp\left(-\frac{\mu_a}{k_B T_m}\right), \tag{3}$$

where $I(T)$ is the TSDC in A; Q_0 is the charge quantity in C; τ_0 is the relaxation time constant in s; u_a is the activation energy of the peak caused by relaxation polarization or the trap depth for the peak caused by traps, in electron volt; γ is the heating rate in K/s; T_0 is the initial temperature in K; and T_m is the peak temperature in K. For the peaks caused by traps, the trap density N_t could be estimated using the following equation:

$$N_t = \frac{Q_0}{eSd}, \tag{4}$$

where e is the elementary charge in C, S is the area of the sample in m^2, and d is the thickness of the sample in m.

In Fig. 4, all the experimental curves were well fitted with Eq. (2) and there are four separate peaks for each sample, which were named as peaks 1, 2, 3, and 4 in order from low temperature to high temperature. Their origins could be based on relevant papers.[44–46] Dipoles dominate at low temperature and correspond to peak 1 and peak 2. In the nanocomposites, interfaces could also contribute to the dipolar polarization. During the process, interface regions will be charged and contain the dipoles, which may be oriented under an applied field. Space charges prevail in the high temperature region and correspond to peak 3 and peak 4.

Shallow and deep trap parameters of the nanocomposites were extracted from peak 3 and peak 4, respectively, as shown in Figs. 5(a) and 5(b). With the increase in the BT content, depths of shallow and deep traps decrease after an initial increase and finally tend to be stable. Moreover, their densities are significantly improved at a high content. For example, the densities of shallow and deep traps of 50 wt. % PI/BT nanocomposites are 1.47×10^{20} m^{-3} and 4.37×10^{19} m^{-3}, which are 84 and 7 times the values of Pure PI, respectively. It is suggested that the changed trapping occurs at the interfaces between BT nanofillers and the PI matrix, which is made up of the bonded, transitional, and normal regions.[32] While the BT content is relatively low, the interaction of the nanoparticles could be disregarded and the interfaces are almost independent, where carriers will be captured by deep traps in the bonded regions. At a higher content of BT, the interfaces are overlapped because of the shorter distance between the nanoparticles and more serious aggregation; hence, the role of deep traps will be limited and more shallow traps will appear, which could assist carriers in bulk transport. Based on the trends shown in Figs. 5(a) and 5(b), the influence of trap parameters on breakdown strength could be reasonably deduced. For the nanocomposites with a low content of BT (range I), the variation of breakdown strength is mainly associated with deep traps. At a higher content of nanoparticles (range II), the breakdown strength is together influenced by shallow and deep traps, especially their depths. While the BT content is much higher (range III), increased shallow trap density becomes the dominant factor of the breakdown strength reduction.

In order to study the influence more clearly, a physical quantity of average trap depth was defined to describe the whole trap properties of the nanocomposites,

$$u_{av} = \frac{u_{a(s)} N_{t(s)} + u_{a(d)} N_{t(d)}}{N_{t(s)} + N_{t(d)}}, \tag{5}$$

where u_{av} is the average trap depth in electron volt; $u_{a(s)}$ and $u_{a(d)}$ are the shallow and deep trap depths, respectively, in electron volt; and $N_{t(s)}$ and $N_{t(d)}$ are the shallow and deep trap densities, respectively, in m^{-3}. As shown in Fig. 5(c), there is a clear corresponding relationship in which a larger average trap depth corresponds to a higher breakdown strength. Compared with the various trap parameters, the average trap depth we defined is a more universal and intrinsic parameter related to conductivity and breakdown strength.

In summary, the breakdown strength and energy density of PI/BT nanocomposites reach maximum values of 520 kV/mm and 4.51 J/cm^3 at 0.05 wt. %, while keeping a good thermal stability (3.22 J/cm^3 at

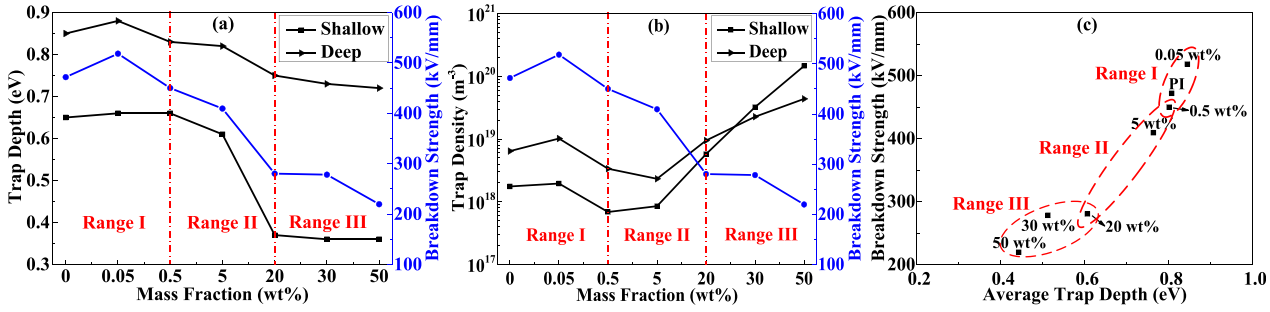

FIG. 5. Relationship between (a) trap depth, (b) trap density, (c) average trap depth, and breakdown strength for PI/BT nanocomposites.

100 °C). Moreover, trap properties and their effect on breakdown strength were studied through TSDC. The dominant trap parameter, with the increase in the BT content, is correlated with deep traps, deep and shallow traps especially their depths, and shallow trap density. Then, it was found that a larger average trap depth corresponds to a higher breakdown strength, the value of which decreases from 0.81 eV to 0.44 eV as the BT content increases to 50 wt. %. This work presents an effective strategy to enhance energy density while maintaining high breakdown strength for PI nanocomposites and provides an understanding of the role of traps in dielectric breakdown. Recently, particle arrangement and symmetry in multilayer PI nanocomposites are receiving increasing attention.[7,14,47] This work also will support future studies on them. For instance, the PI nanocomposite with 0.05 wt. % of BT could be used as the "insulation layer" instead of pure PI in a multilayer structure design, and the calculated trap parameters could be used for charge transport and breakdown behavior simulation in the multilayer samples. Moreover, the PI composite filled with in-plane aligned 1D nanofillers is also an interesting direction.

See the supplementary material for FTIR spectra, XRD patterns, and TEM and SEM images of BT nanoparticles, pure PI, and PI/BT nanocomposites.

This work was supported by the National Basic Research Program of China (Grant No. 2015CB251003) and the National Natural Science Foundation of China (Grant Nos. U1830131 and 11575140). J. Ru gratefully acknowledges the financial support from China Scholarship Council.

REFERENCES

[1]D. Tan, L. L. Zhang, Q. Chen, and P. Irwin, J. Electron. Mater. **43**(12), 4569 (2014).
[2]W. J. Sarjeant, I. W. Clelland, and R. A. Price, Proc. IEEE **89**(6), 846 (2001).
[3]Y. Cao, P. C. Irwin, and K. Younsi, IEEE Trans. Dielectr. Electr. Insul. **11**(5), 797 (2004).
[4]P. Barber, S. Balasubramanian, Y. Anguchamy, S. S. Gong, A. Wibowo, H. S. Gao, H. J. Ploehn, and H. C. zur Loye, Materials **2**(4), 1697 (2009).
[5]Q. Chen, Y. Shen, S. H. Zhang, and Q. M. Zhang, Annu. Rev. Mater. Res. **45**, 433 (2015).
[6]X. Zhang, Y. Shen, Q. H. Zhang, L. Gu, Y. H. Hu, J. W. Du, Y. H. Lin, and C. W. Nan, Adv. Mater. **27**(5), 819 (2015).
[7]Y. F. Wang, L. X. Wang, Q. B. Yuan, J. Chen, Y. J. Niu, X. W. Xu, Y. T. Cheng, B. Yao, Q. Wang, and H. Wang, Nano Energy **44**, 364 (2018).
[8]Z. M. Dang, Y. Q. Lin, H. P. Xu, C. Y. Shi, S. T. Li, and J. B. Bai, Adv. Funct. Mater. **18**(10), 1509 (2008).
[9]B. H. Fan, J. W. Zha, D. R. Wang, J. Zhao, and Z. M. Dang, Appl. Phys. Lett. **100**(9), 092903 (2012).
[10]C. W. Beier, J. M. Sanders, and R. L. Brutchey, J. Phys. Chem. C **117**(14), 6958 (2013).
[11]Q. G. Chi, J. Sun, C. H. Zhang, G. Liu, J. Q. Lin, Y. N. Wang, X. Wang, and Q. Q. Lei, J. Mater. Chem. C **2**(1), 172 (2014).
[12]X. W. Peng, Q. Wu, S. H. Jiang, M. Hanif, S. L. Chen, and H. Q. Hou, Mater. Lett. **133**, 240 (2014).
[13]H. Liu, P. Xu, H. B. Yao, W. H. Chen, J. Y. Zhao, C. Q. Kang, Z. Bian, L. X. Gao, and H. Q. Guo, Appl. Surf. Sci. **420**, 390 (2017).
[14]Y. Q. Chen, B. P. Lin, X. Q. Zhang, J. C. Wang, C. W. Lai, Y. Sun, Y. R. Liu, and H. Yang, J. Mater. Chem. A **2**(34), 14118 (2014).
[15]W. H. Xu, Y. C. Ding, S. H. Jiang, L. L. Chen, X. J. Liao, and H. Q. Hou, Mater. Lett. **135**, 158 (2014).
[16]J. N. Liu, G. F. Tian, S. L. Qi, Z. P. Wu, and D. Z. Wu, Mater. Lett. **124**, 117 (2014).
[17]Y. Yang, H. L. Sun, B. P. Zhu, Z. Y. Wang, J. H. Wei, R. Xiong, J. Shi, Z. Y. Liu, and Q. Q. Lei, Appl. Phys. Lett. **106**(1), 012902 (2015).
[18]Y. Yang, H. L. Sun, D. Yin, Z. H. Lu, J. H. Wei, R. Xiong, J. Shi, Z. Y. Wang, Z. Y. Liu, and Q. Q. Lei, J. Mater. Chem. A **3**(9), 4916 (2015).
[19]Y. C. Zhou and H. Wang, Appl. Phys. Lett. **102**(13), 132901 (2013).
[20]J. C. Wang, Y. C. Long, Y. Sun, X. Q. Zhang, H. Yang, and B. P. Lin, Appl. Surf. Sci. **426**, 437 (2017).
[21]W. W. Wang, D. M. Min, and S. T. Li, IEEE Trans. Dielectr. Electr. Insul. **23**(1), 564 (2016).
[22]S. M. Peng, J. L. He, J. Hu, X. Y. Huang, and P. K. Jiang, IEEE Trans. Dielectr. Electr. Insul. **22**(3), 1512 (2015).
[23]S. T. Li, D. M. Min, W. W. Wang, and G. Chen, IEEE Trans. Dielectr. Electr. Insul. **23**(5), 2777 (2016).
[24]P. H. Hu, Y. Shen, Y. H. Guan, X. H. Zhang, Y. H. Lin, Q. M. Zhang, and C. W. Nan, Adv. Funct. Mater. **24**(21), 3172 (2014).
[25]P. H. Hu, W. D. Sun, M. Z. Fan, J. F. Qian, J. Y. Jiang, Z. K. Dan, Y. H. Lin, C. W. Nan, M. Li, and Y. Shen, Appl. Surf. Sci. **458**, 743 (2018).
[26]X. Zhang, Y. Shen, B. Xu, Q. H. Zhang, L. Gu, J. Y. Jiang, J. Ma, Y. H. Lin, and C. W. Nan, Adv. Mater. **28**(10), 2055 (2016).
[27]B. Xie, H. B. Zhang, Q. Zhang, J. D. Zang, C. Yang, Q. P. Wang, M. Y. Li, and S. L. Jiang, J. Mater. Chem. A **5**(13), 6070 (2017).
[28]N. Z. Bao, L. M. Shen, A. Gupta, A. Tatarenko, G. Srinivasan, and K. Yanagisawa, Appl. Phys. Lett. **94**(25), 253109 (2009).
[29]K. Kenry and C. T. Lim, Prog. Polym. Sci. **70**, 1 (2017).
[30]L. Y. Liang, X. L. Kang, Y. H. Sang, and H. Liu, Adv. Sci. **3**(7), 1500358 (2016).
[31]Y. Zhang, C. H. Zhang, Y. Feng, T. D. Zhang, Q. G. Chen, Q. G. Chi, L. Z. Liu, G. F. Li, Y. Cui, X. Wang, Z. M. Dang, and Q. Q. Lei, Nano Energy **56**, 138 (2019).
[32]S. T. Li, G. L. Yin, G. Chen, J. Y. Li, S. N. Bai, L. S. Zhong, Y. X. Zhang, and Q. Q. Lei, IEEE Trans. Dielectr. Electr. Insul. **17**(5), 1523 (2010).
[33]P. Bräunlich, *Thermally Stimulated Relaxation in Solids* (Springer-Verlag, Berlin, 1979).
[34]Y. Wang, Y. F. Hou, and Y. Deng, Compos. Sci. Technol. **145**, 71 (2017).
[35]S. Chisca, V. E. Musteata, I. Sava, and M. Bruma, Eur. Polym. J. **47**(5), 1186 (2011).
[36]D. M. Min, C. Y. Yan, R. Mi, C. Ma, Y. Huang, S. T. Li, Q. Z. Wu, and Z. L. Xing, Polymers **10**(11), 1207 (2018).
[37]J. P. Calame, J. Appl. Phys. **99**(8), 084101 (2006).
[38]L. An, S. A. Boggs, and J. P. Calame, IEEE Electr. Insul. Mag. **24**(3), 5 (2008).
[39]W. D. Sun, X. J. Lu, J. Y. Jiang, X. Zhang, P. H. Hu, M. Li, Y. H. Lin, C. W. Nan, and Y. Shen, J. Appl. Phys. **121**(24), 244101 (2017).
[40]M. Wang, W. L. Li, Y. Feng, Y. F. Hou, T. D. Zhang, W. D. Fei, and J. H. Yin, Ceram. Int. **41**(10), 13582 (2015).
[41]J. C. Wang, Y. C. Long, Y. Sun, X. Q. Zhang, H. Yang, and B. P. Lin, J. Mater. Sci.: Mater. Electron. **29**(9), 7842 (2018).
[42]S. S. Yue, B. Q. Wan, H. Y. Li, Y. Y. Liu, and Q. W. Zhang, Int. J. Electrochem. Sci. **14**, 2049 (2019).
[43]R. Chen, J. Mater. Sci. **11**(8), 1521 (1976).
[44]R. P. Bhardwaj, J. K. Quamara, B. L. Sharma, and K. K. Nagpaul, J. Phys. D: Appl. Phys. **17**(5), 1013 (1984).
[45]Y. Fan, X. Wang, W. G. Zhang, and Q. Q. Lei, J. Phys. D: Appl. Phys. **32**(21), 2809 (1999).
[46]R. Lal, B. S. Rathore, and M. S. Gaur, Ionics **18**(6), 565 (2012).
[47]G. R. Chen, J. Q. Lin, X. Wang, W. L. Yang, D. P. Li, W. M. Ding, H. D. Li, and Q. Q. Lei, J. Mater. Sci.: Mater. Electron. **28**(18), 13861 (2017).